

Design of nanofibre interlayer supported forward osmosis composite membranes and its evaluation in fouling study with cleaning

Tao Ma¹, Haiqing Hui¹, Xiaofei You², Zhiqiang Pei³, Miao Tian (✉)¹, Bing Wu⁴

¹ School of Ecology and Environment, Northwestern Polytechnical University, Xi'an 710072, China

² Singapore Membrane Technology Centre, Nanyang Environment and Water Research Institute, Nanyang Technological University, Singapore 637141, Singapore

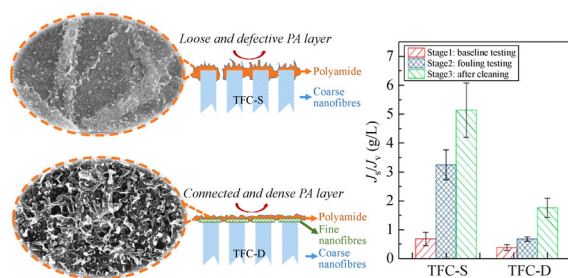
³ Beijing Origin Water Membrane Technology Co., Ltd., Beijing 101407, China

⁴ Faculty of Civil and Environmental Engineering, University of Iceland, Reykjavik IS-107, Iceland

HIGHLIGHTS

- A fine fibre (40–60 nm diameter) interlayer (~1 μm thickness) was electrospun.
- Fine fibre interlayer promoted formation of defect-free dense polyamide layer.
- FO membrane with dual-layer substrate had less organic fouling potential.
- High reverse salt flux accelerated organic fouling on FO membrane.

GRAPHIC ABSTRACT



ARTICLE INFO

Article history:

Received 6 October 2021

Revised 23 December 2021

Accepted 2 January 2022

Available online 25 February 2022

Keywords:

Forward osmosis
Electro-spinning
Interfacial polymerisation
Fouling
Polyvinylidene fluoride

ABSTRACT

Nanofibre-supported forward osmosis (FO) membranes have gained popularity owing to their low structural parameters and high water flux. However, the nanofibrous membranes are less stable in long-term use, and their fouling behaviours with foulants in both feed solution (FS) and draw solution (DS) is less studied. This study developed a nanofibrous thin-film composite (TFC) FO membrane by designing a tiered dual-layer nanofibrous substrate to enhance membrane stability during long-term usage and cleaning. Various characterisation methods were used to study the effect of the electrospun nanofibre interlayer and drying time, which is the interval after removing the M-phenylenediamine (MPD) solution and before reacting with trimesoyl chloride (TMC) solution, on the intrinsic separation FO performance. The separation performance of the dual-layer nanofibrous FO membranes was examined using model foulants (sodium alginate and bovine serum albumin) in both the FS and DS. The dual-layer nanofibrous substrate was superior to the single-layer nanofibrous substrate and showed a flux of 30.2 L/m²/h (LMH) when using 1.5 mol/L NaCl against deionised (DI) water in the active layer facing draw solution (AL-DS) mode. In the fouling test, the water flux was effectively improved without sacrificing the water/solute selectivity under the condition that foulants existed in both the FS and DS. In addition, the dual-layer nanofibrous TFC FO membrane was more robust during the fouling test and cleaning.

© Higher Education Press 2022

1 Introduction

Industrialisation and urbanisation have led to severe water pollution and shortage of drinking water resources (Jones et al., 2019). Recycling wastewater for non-potable use is

considered a feasible solution, and has attracted attention in recent decades (Manju and Sagar, 2017; Tang et al., 2018). Membrane technology has been extensively utilised in purifying wastewater complexes because of its small footprint, high-quality permeate, low cost, and easy integration with other technologies (Nasrul et al., 2011; Ali et al., 2018; Xiao et al., 2019). An emerging membrane-based technology, forward osmosis (FO), uses natural energy and osmotic pressure gradient as the driving

✉ Corresponding author

E-mail: mtian@nwpu.edu.cn

forces to separate water from target wastewater streams (Xu et al., 2017). Water naturally permeates through a semi-permeable membrane from the feed solution (FS) side with low osmotic pressure to the draw solution (DS) side with high osmotic pressure, while the solute is retained in the FS (Martinetti et al., 2009; Zhang et al., 2010).

Compared with pressurised membrane technologies such as microfiltration (MF), ultrafiltration (UF), nanofiltration (NF), and reverse osmosis (RO), the FO process does not require external pressure, resulting in low energy consumption and low membrane fouling potential (Cath et al., 2006). Although the FO technology is widely recognised in RO pre-treatment, wastewater treatment, brine dilution, food flavour concentration, and other water treatment fields (Sreedhar et al., 2018; Suwaileh et al., 2020; Abdullah et al., 2021; Wang et al., 2021; Zhang et al., 2021), the large-scale application of FO is hindered by the lack of high-performance FO membranes (Blandin et al., 2020; Yadav et al., 2020). It has been demonstrated that an ideal high-performance FO membrane should have high water permeability, low salt permeability, low structural parameter (*S* value), excellent antifouling performance, and stable chemical properties (Wang et al., 2010; Tian et al., 2017).

Generally, thin-film composite (TFC) FO membranes composed of porous substrates and ultra-thin polyamide (PA) selective layers display structural design flexibility and superior permeability and selectivity compared to symmetric cellulose triacetate (CTA) FO membranes (Klaysom et al., 2013; Liu et al., 2016; Yang et al., 2019). However, there is still room for further improvements in the water permeability and selectivity of TFC membranes, such as overcoming the ‘trade-off’ between water permeability and solute selectivity. Recent work has shown that constructing a hydrophilic, highly porous, small pore-sized nano-interlayer between the substrate and function layer can simultaneously improve the water flux and reduce the back solute flux in the FO process (Zhou et al., 2018; Deng et al., 2020; Yang et al., 2020; Zhang et al., 2020; Li et al., 2021b). These highly porous hydrophilic interlayers could impede the transport of *m*-phenylenediamine (MPD) to the reaction interface with trimesoyl chloride (TMC), resulting in a thin and superior permeable PA layer (Zhang et al., 2019). In addition to constructing nano-interlayers on the polymer matrix to promote the formation of defect-free polyamide based selective layer, the TiO₂ nano-interlayers on the coarse mullite ceramic substrate facilitated the growth of a thin well-connected metal-organic framework (MOF, UiO-66) nanoporous selective layer through secondary growth, and the MOF selective layer showed an almost complete salt rejection (99.9%), good anti-fouling performance, and high long-term stability in harsh environments (Li et al., 2021a). A well-connected MOF selective layer membrane provides a possibility to prepare pure inorganic FO

membranes. It is expected that this method can be extended to solvent-resistant FO membranes in the future. As mentioned above, most interlayers were deposited on a porous substrate fabricated via non-solvent induced phase separation (NIPS) with low porosity. Thus, the overall *S* value of FO membranes was not minimised, which could lead to internal concentration polarisation (ICP) and membrane fouling during long-term FO operation (McCutcheon and Elimelech, 2006; Wang et al., 2014; Wang et al., 2016).

In recent years, electro-spinning nanofibre-supported TFC FO membranes have become popular (Saleem et al., 2020). It has been well documented that electrospinning can produce nanofibres with large specific surface areas, high porosities, and fully active pore structures, which alleviate ICP and enhance the water flux. Additionally, researchers have explored ways to further improve the water flux by modifying the nanofibre substrates, such as coating polyvinyl alcohol to improve the hydrophilicity of the substrates (Park et al., 2018) and introducing graphene oxide and oxidised multi-walled carbon nanotube interlayers (Yu et al., 2020). Polyvinylidene fluoride (PVDF) is a semi-crystalline polymer with repeating units, which is widely used to prepare membrane materials for water treatment because of its strong mechanical properties and stable chemical properties. Additionally, the preparation of a defect-free and robust PA separation layer on the electro-spinning nanofibrous substrate (particularly PVDF) with large open surface pores via interfacial polymerisation is a key process (Tian et al., 2013). Thus, the development of robust electro-spinning nanofibre-based FO membranes is necessary. Our previous study reported that a smaller fibre (~150 nm) would stimulate a denser and defect-free PA layer on a hydrophilic polyetherimide nanofibrous substrate (Tian et al., 2015). It is possible that the nano-interlayers with smaller diameters can further promote the formation of a highly permeable and defect-free PA layer.

On the other hand, although the selective layer of FO membranes is generally placed against feed wastewater (Zhang et al., 2019; Kim et al., 2020; Luo et al., 2021), the membrane substrate structure could still affect the FO membrane performance if the DS (facing support layer) contains potential foulants (Qasim et al., 2015; Gao et al., 2017; Xue et al., 2020). Thus, the influence of the physical and chemical properties of the TFC FO membrane on fouling needs to be studied when both FS and DS contain potential foulants. A highly porous substrate with an interconnected open pore structure is expected to be one of the most feasible and accessible strategies to alleviate the ICP phenomenon and membrane fouling in FO.

Here, we report the design of a dual-layer-structured PVDF nanofibre-supported TFC FO membrane. The nanofibrous substrate consists of a non-woven support layer, a coarse fibre layer (100–300 nm), and a fine fibre interlayer (40–60 nm). The influence of fibre morphology and drying duration before the reaction with TMC on the

formation of the PA selective layer was also investigated. The fine fibre interlayer was expected to stimulate the formation of a more robust, dense, and defect-free PA layer. In addition, using typical polysaccharides (sodium alginate, SA) and proteins (bovine serum albumin, BSA), we analysed the influence of the substrate pore structure on the fouling behaviour of foulants in both FS and DS. Our results reveal the behaviour of foulants on the membrane surface and provide a theoretical basis for the research and development of high water flux and anti-pollution TFC FO membranes in actual wastewater treatment.

2 Materials and methods

2.1 Membrane materials and chemicals

Unless otherwise specified, all chemicals were used as received without further purification. A non-woven mesh substrate (Grade 3233) was purchased from Ahlstrom (USA). The nanofibrous substrates were prepared using PVDF (Kynar® HSV900, Arkema, Singapore). N, N-dimethylformamide (DMF, CAS: 68-12-2, $\geq 99.5\%$, Sinopharm, China) and acetone (CAS: 67-64-1, $\geq 99.5\%$, Sinopharm, China) were used as solvents for preparing the PVDF dope solution. Lithium chloride (CAS: 7447-41-8, $\geq 99.0\%$) was purchased from Aladdin Biochemical Technology Co., Ltd (China). TMC (CAS: 4422-95-1, 98%, Aladdin Biochemical Technology Co., Ltd, China) and MPD (CAS: 108-45-2, $\geq 99.5\%$, Sinopharm, China) were used for the PA layer formation. Deionised (DI) water with a resistivity of $18.2 \text{ M}\Omega \cdot \text{cm}$ (Millipore Integral 10 Water Purification System, China) was used to prepare all the aqueous solutions. SA (CAS: 9005-38-3, Sinopharm, China) and BSA (CAS: 9048-46-8, Sinopharm, China) were used as foulants. A commercial CTA FO membrane, purchased from Hydration Technology Innovations (HTI, Albany, USA), was used as a benchmark.

2.2 Preparation of PVDF nanofibre substrates

The nanofibrous substrates were fabricated as described previously (Tian et al., 2017). In brief, the required amount of PVDF powder was dissolved in DMF/acetone (6:4 v/v) at 70°C . Two types of nanofibrous substrates were developed: Sub-S and Sub-D. The substrate Sub-S consisted of a single-layer nanofibre and was fabricated via 8.0 wt% PVDF solution, whereas the substrate Sub-D consisted of a dual-layer nanofibre and was prepared with two dope solutions. All nanofibrous substrate layers were kept in a ventilated fume hood overnight to remove residual solvent before being hot-pressed at 155°C for 1 h. The detailed dope formulation and electrospinning parameters of the nanofibrous substrate layer are summarised in Table 1.

Table 1 Electrospinning conditions for preparation of the nanofibre substrates

Parameters	Sub-S	Sub-D	
	Homogeneous	Top	Bottom
PVDF (wt%)	8	5	8
Solvent	DMF/acetone	DMF/acetone	DMF/acetone
Flow rate ($\mu\text{L}/\text{min}$)	80	50	80
Applied voltage (kV)	19 ± 1	21 ± 1	19 ± 1
Working distance (cm)	12	12	12
Humidity (%)	60 ± 2	50 ± 2	60 ± 2

2.3 Synthesis of PA selective layer on nanofibrous substrates

The nanofibrous substrates were first pre-wet with ethanol, washed with DI water, and stored in DI water at 4°C for further use. Then, the PA selective layer was synthesised on top of a nanofibrous substrate by interfacial polymerisation (IP) using TMC and MPD as monomers. The substrate was fixed in a frame, and 2.0 wt% MPD aqueous solution was poured onto the nanofibrous substrate for a contact time of 5 min. The excess solution was then carefully removed using a rubber roller. The drying duration meant that the membrane was kept in air after removing the MPD droplets using a rubber roller. Then, 0.1 w/v% TMC was introduced to the membrane surface to react with MPD for 1 min to form the PA selective layer. The fabricated membranes were then coded as TFC-S-*X* and TFC-D-*X*, where which S represented a single layer, D represented a double layer, and *X* represented the drying duration.

2.4 Membrane characterization

Prior to the observation under a field emission scanning electron microscope (FESEM) (Verios G4, FEI, USA), all samples were sputtered with platinum using a sputter coater (Hitachi MC1000, Japan) at 20 mA for 60 s. For cross-sectional observation, the sample was prepared by freeze-fracturing in liquid nitrogen. An image analysis software based on the FESEM images was used to measure the fibre diameter. The actual membrane thickness was measured using a digital micrometre (Aladdin M3176-01, China). Atomic force microscopy (AFM) (Dimension Icon, Bruker, Germany) was used to estimate the surface roughness of the TFC membranes. The hydrophilicity of the membrane surface was assessed using contact angle measurements (DSA25, KRUSS, Germany). The porosity of the membrane was calculated through gravimetric analysis. In addition, the organic foulants on the membrane surface were characterised using a TOC analyser (Island ferry TOC-LCPH, Japan). In brief, the fouled membrane

(2 cm × 3 cm) was placed into a tube with 15 mL DI water and shaken for 30 min. The cleaning solution was collected for TOC analysis.

2.5 Membrane performance evaluation

The water flux and reverse salt flux of the TFC FO membrane were studied in a lab-scale FO system, as described previously (Tian et al., 2013). The membrane cell had an effective area of 24 cm² (4 cm in width and 6 cm in length). The FO membranes were operated in the AL-DS mode using 1.5 mol/L NaCl solution as the DS (crossflow velocity of 17.9 cm/s) and DI water as FS (crossflow velocity of 17.9 cm/s). The water flux and reverse salt flux were examined by monitoring the weight and conductivity of the FS. The *S* value of the substrate was calculated following the protocol described in our previous study (Tian et al., 2013).

In addition, the water permeability coefficient (*A*, L/m²/h/bar), solute rejection rate (*R*, %), and salt permeability coefficient (*B*, L/m²/h) of the FO membranes were evaluated using a reverse osmosis (RO) membrane system (1.5 bar, 42 cm², 200 mg/L NaCl).

2.6 Organic fouling experiments

To evaluate the fouling potential of the nanofibre support layer, organic fouling was tested in a lab-scale FO system running in the AL-DS mode (crossflow velocity of 17.9 cm/s for both FS and DS). The FO experiment consisted of three stages. In the first stage, the intrinsic FO membrane performance was evaluated with 1.5 mol/L NaCl as DS (1 L) and DI water as FS (1 L) for 0.5 h to obtain the baseline water flux, J_b^t (LMH). Subsequently, 200 mg/L of model foulant (SA) was added to the FS and DS. The FO performance testing lasted for 5 h, and the final water flux was represented as J_w^t (i.e., stage 2). Then, DI water was used as FS and 1.5 mol/L NaCl as DS to clean the membrane for 60 min, and the obtained water flux was termed J_c^t (i.e., stage 3). To evaluate the antifouling performance of the membranes, the flux recovery ratio (FRR) was calculated using Eq. (1);

$$\text{FRR} = \frac{J_c^t}{J_b^t} \quad (1)$$

At the end of stage 3, the fouled membrane (2 cm × 3 cm) was placed in a 15 mL DI water tube and shaken for 30 min. The foulant solution was collected and filtered with a 0.45 μm filter before TOC analysis.

3 Results and discussion

3.1 Characteristics of nanofibrous substrates

To enhance the selectivity and mechanical stability of the

PA layer formed on the hydrophobic PVDF nanofibrous substrate, a nanofibre interlayer on top of a coarse nanofibre layer was designed to promote the formation of a defect-free PA layer. The Sub-D substrate consisted of two layers of PVDF nanofibres, and the morphology is illustrated in Fig. 1. The cross-sectional FESEM image in Fig. 1(a) shows that the substrate consisted of a dual nanofibre layer, ~1 μm of fine nanofibres and ~30 μm of coarse nanofibres. The cross-sectional FESEM image (Fig. 1(b)) shows that a PA layer was formed on the top fine nanofibre layer of Sub-D. The image (Fig. 1(c)) shows that the diameter of the top fine nanofibres of Sub-D fabricated with a 5.0 wt% PVDF solution ranged between 40–60 nm (Fig. 1(d)). In contrast, as shown in Figs. 1(e) and 1(f), the diameter of the coarse fibre of Sub-S, fabricated with 8.0 wt% PVDF solution, was mostly in the range of 150–300 nm. This shows that the fibre diameter could be effectively reduced by decreasing the polymer dope concentration, which facilitated the acceleration of the electrostatic drawing of the jet.

The characteristics of the Sub-S and Sub-D nanofibrous substrates are summarised in Table 2. Sub-S and Sub-D had no significant differences in thickness and contact angle. The mean pore sizes of substrates Sub-S and Sub-D were 0.92±0.01 and 0.54±0.06 μm, respectively. The porosities of Sub-S and Sub-D were 70.5%±2.2% and 60.2%±5.0%, respectively. The addition of an interlayer reduced the membrane pore size and porosity.

3.2 Morphology of the TFC FO membranes

The fine nanofibre diameters of the Sub-D surface were in the range of 40–60 nm, and the coarse nanofibre diameters on the Sub-S surface were in the range of 150–300 nm, as evidenced by FESEM. The influence of the nanofibre diameter on the formation of the PA layer by IP was investigated, and the results are shown in Fig 2. Low-magnification FESEM images are shown in Figs. 2(a)–2(d), while high-magnification FESEM images are shown in Figs. 2(e)–2(h). The results showed that a typical PA layer of ridges and valleys was successfully formed on both substrates and it covered the gaps between the nanofibres. The open area between the coarse nanofibres was quite large, and fibres under the PA layer were visible (Figs. 2(a), 2(b), 2(e), and 2(f)). In contrast, the open area between the fine nanofibres was relatively small, and the PA layer covered the entire nanofibre (Figs. 2(c), 2(d), 2(g), and 2(h)). It was observed that the PA synthesised on Sub-D with a smaller fibre diameter had a uniform leaf-like structure, whereas the PA formed on the coarse fibre had two different structures: a flatter surface between the nanofibres and a rough leaf-like structure near the nanofibres. A flat PA was formed due to the insufficient storage of MPD monomers between the coarse nanofibres, which inhibited leaf-like features and resulted in a flatter PA layer.

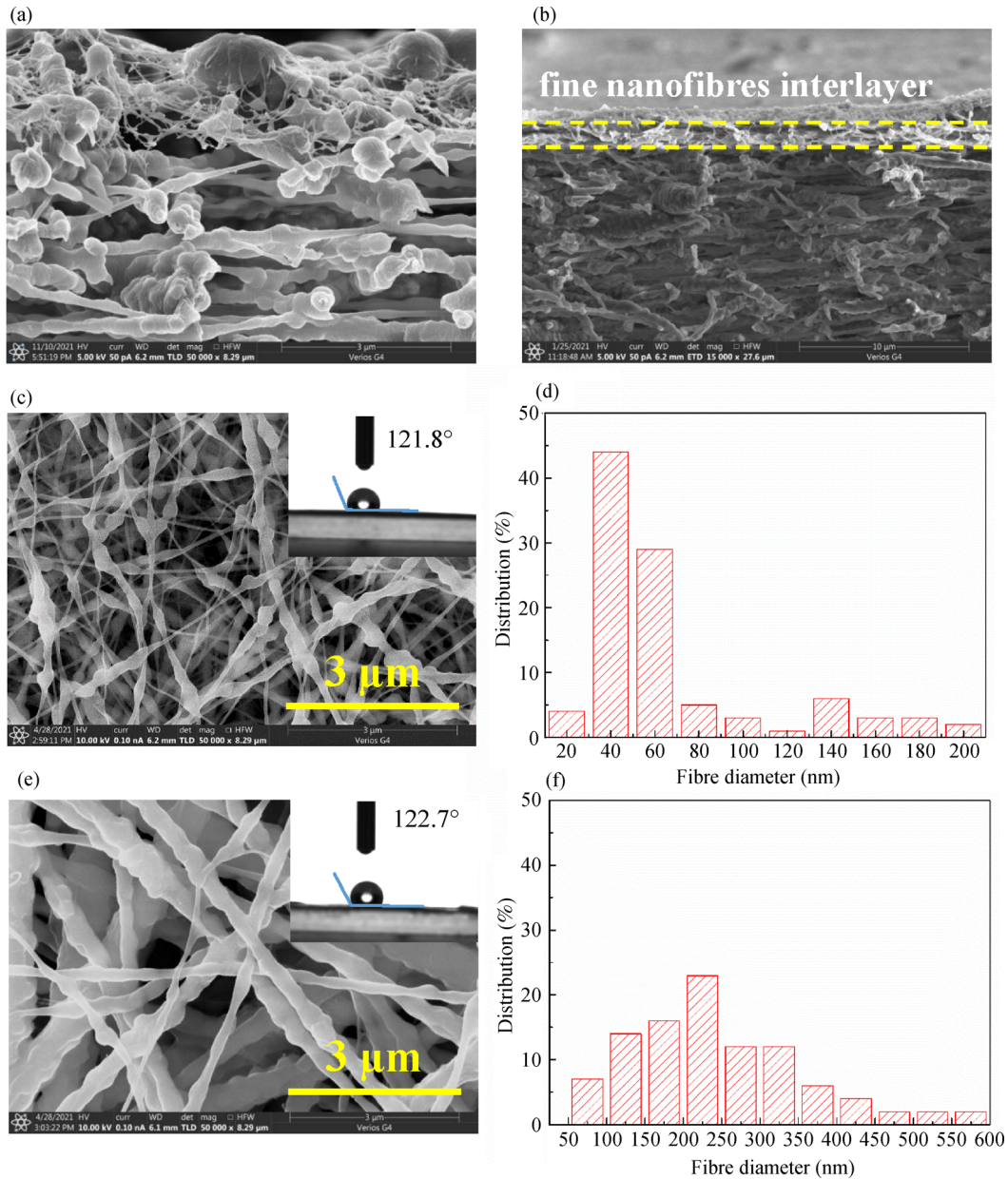


Fig. 1 FESEM images of electrospinning PVDF nanofibre substrates. (a) Cross-sectional view of Sub-D; (b) Cross-sectional view after IP of Sub-D; (c) Surface morphology and (d) fibre diameter distribution of the nanofibre layer fabricated with 5.0 wt% PVDF; (e) Surface morphology and (f) fibre diameter distribution of the nanofibre layer fabricated with 8.0 wt% PVDF.

Table 2 Properties of Sub-S and Sub-D nanofibrous substrates (The error bars were calculated based on at least three independently repeated tests)

Parameter	Sub-S	Sub-D
Membrane thickness (μm)	33.8 ± 0.3	31.1 ± 0.6
Contact angle ($^\circ$)	122.7 ± 3.3	121.8 ± 6.3
Porosity (%)	70.5 ± 2.2	60.2 ± 5.0
Mean pore size (μm)	0.92 ± 0.01	0.54 ± 0.06
Max pore size (μm)	1.35 ± 0.14	0.81 ± 0.04

It has been reported that the hydrophobicity of the substrate is likely to reduce MPD uptake and inhibit the formation of leaf-like patterns due to a reduced capillary effect (Peng et al., 2020). Our results demonstrated that in addition to the chemical properties of the substrate, the pore structure of the substrate could also influence MPD absorption and promote leaf-like patterns, which is of great significance for the formation of a PA layer on an inert hydrophobic material. Thus, the finer nanofibre was likely to increase MPD uptake by the substrate and induce the formation of leaf-like roughness features. In addition, the

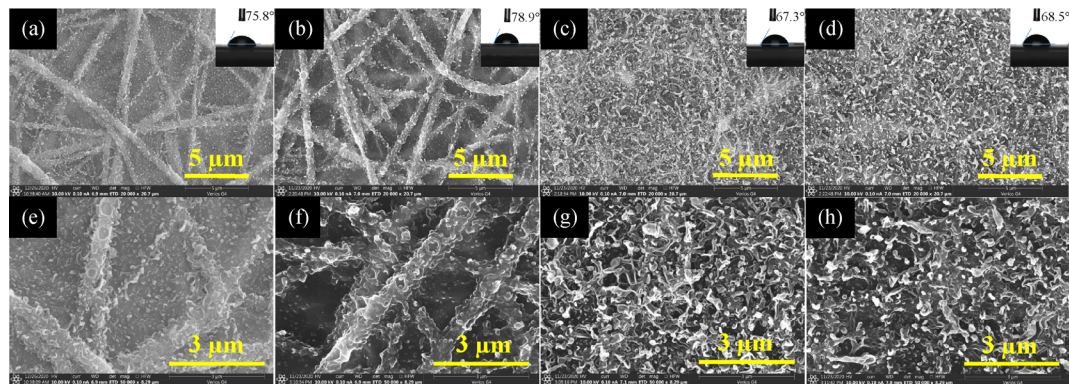


Fig. 2 Low-magnification and high-magnification FESEM images of the PA surface of the composite membranes, (a, e) TFC-S-1; (b, f) TFC-S-2; (c, g) TFC-D-1; (d, h) TFC-D-2. Note that TFC-S-1 refers to the TFC membrane fabricated on the nanofibrous substrate Sub-S, and the drying duration was 1 min.

drying duration of the aqueous phase in the nanofibrous substrate was expected to influence the reaction interface between the MPD and TMC monomers and the integration strength between the nanofibres and PA (Lau et al., 2012). Additionally, as evidenced by the FESEM images (Fig. 2), extending the drying duration from 1 to 2 min lowered the reaction interface and improved the visibility of the coarse nanofibre pattern (Fig. 2(e) vs. 2(f)).

The inset images show the contact angles of each membrane (Fig. 2). The contact angles of TFC-S-1, TFC-S-2, TFC-D-1, and TFC-D-2 were 75.8°, 78.9°, 67.3°, and 68.5°, respectively. According to the Wenzel equation, the measured water contact angle is related to the surface roughness (Wenzel, 1949). However, experiments have shown that PA (Extrand, 2004) and polyethylene (Holmes-Farley et al., 1985) surfaces with consistent surface chemical compositions exhibit contact angles independent of surface roughness. There is no consensus on the correlation between the roughness and contact angle. We speculated that the change in the water contact angle of PA may be attributed to the change in the chemical functionality. It has been shown that the contact angle decreases with an increase in amide content (Extrand, 2002). As the PA formed on coarse nanofibres (TFC-S-1 and TFC-S-2) had a lower density and less amide composition, it may have resulted in a higher contact angle.

The membrane surface topography was further characterised using AFM, and the results are shown in Fig. 3. The PA fabricated with a 2 min drying time had a larger histogram depth, which indicated a lower reaction interface. This is consistent with our previous predictions. In addition, the overall depth of PA on coarse fibres was larger than that on fine fibres, indicating a lower reaction interface with coarse fibres. The specific order of the values was TFC-S-2 (1094.1 ± 189.9 nm) > TFC-S-1 (889.8 ± 170.1 nm) > TFC-D-2 (815.7 ± 149.5 nm) > TFC-D-1 (689.5 ± 39.6 nm).

3.3 Performance of FO membranes

The performance of the fabricated FO membranes was tested and compared with that of commercial HTI membranes. All the experiments were conducted in the AL-DS orientation using a 1.5 mol/L NaCl DS against DI water. TFC-S-1 and TFC-S-2 showed significantly higher water flux than the commercial HTI membranes, possibly because of the interconnected open-pore structures, high porosity, and low tortuosity of the nanofibrous substrates. In addition, the dual-layer TFC membranes showed a lower water flux than the single-layer membranes because of the additional resistance of the ultrafine nanofibre layer. However, TFC-S-1 and TFC-S-2 also showed relatively higher reverse salt fluxes than the TFC-D-1, TFC-D-2, and commercial HTI membranes. This was due to the relatively loose PA layer formed on the large opening between the coarse nanofibres. The loose selective layer allowed more salt to diffuse through the membrane, resulting in a higher J_S/J_V value (~ 0.7 g/L), as shown in Fig. 4. It is worth noting that the J_S/J_V value of TFC-D-1 was ~ 0.3 g/L, displaying the best performance among the tested membranes. The above results further confirmed that the fine nanofibre interlayer increased the MPD uptake and promoted the formation of a dense PA layer, inhibiting the reverse diffusion of salt. Figure 5 illustrates the formation of the PA layer on Sub-S and Sub-D, which showed that the loose selective layer on TFC-S had more defects as compared to TFC-D.

The intrinsic separation properties of the selective layer determined by the RO test are described in Table 3, confirming that the PA synthesised on the fine nanofibre interlayer had a higher salt rejection. The A value of HTI was 0.12 LMH/bar, and the values of TFC-S-1 and TFC-S-2 were 0.93 and 0.56 LMH/bar, respectively. The salt rejection of TFC-S-1, TFC-S-2, and HTI was in the range of 40%–60%, showing comparable salt rejection properties. The salt rejection rates of TFC-D-1 and TFC-D-2 were

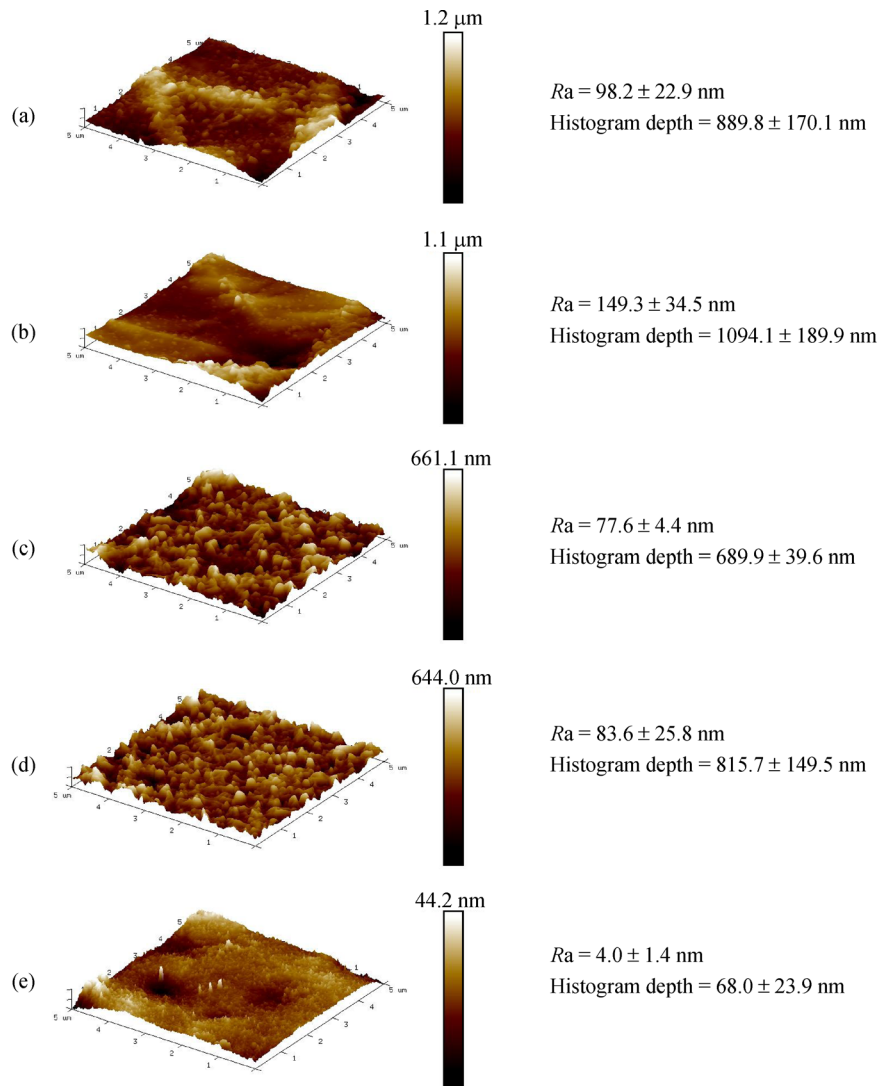


Fig. 3 Typical AFM images of (a) TFC-S-1, (b) TFC-S-2, (c) TFC-D-1, (d) TFC-D-2, and (e) HTI. Histogram depth represents the distance between the highest and lowest point in the scanned area. The error bars were calculated based on four independent replicate tests.

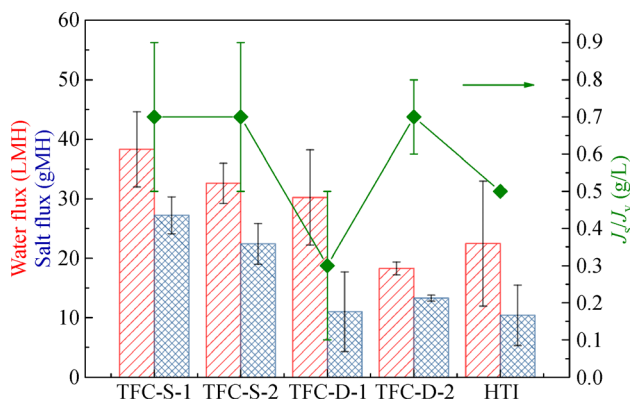


Fig. 4 FO performance of the commercial HTI and prepared TFC membranes operated under the AL-DS mode with 1.5 mol/L NaCl as the DS and DI water as the FS. The error bars were calculated based on 2–3 independent replicate tests.

71% and 77%, respectively. As expected, even at a thickness of ~ 1 μm , the interlayer significantly increased the S value of the substrate from ~ 500 to 1100 μm . The dependence of the water flux of TFC-D-1 on the concentration of DS ranged from 0.5 to 1.5 mol/L NaCl solution against DI water, as illustrated in Fig. S1. Although the presence of fine nanofibres can lead to an increase in the S value, it can also promote the formation of a dense PA layer, thereby reducing the reverse salt flux. In this study, we tried to assess the influence of nanofibre morphology on the permeation selectivity of FO membranes and to improve the salt rejection rate and long-term stability of the membrane at the expense of the S value.

3.4 Organic fouling evaluation

The fouling behaviour of TFC-S-1, TFC-S-2, TFC-D-1, TFC-D-2, and HTI were evaluated in the AL-DS mode

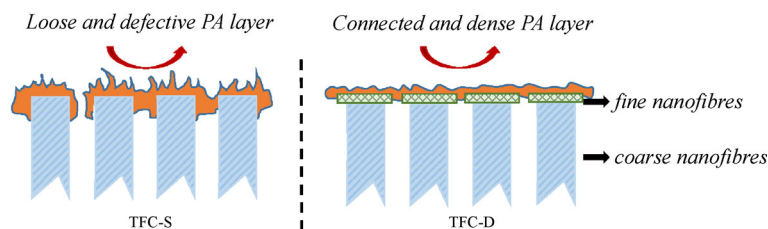


Fig. 5 Schematic of PA layer growing on Sub-S and Sub-D. Fine nanofibres can promote the formation of connected and deflection-free PA layers.

Table 3 Intrinsic separation properties and S values of the FO membranes

Membrane type	Water permeability coefficient, A (L/m ² /h/bar)	Salt permeability coefficient, B (L/m ² /h)	Salt rejection, R (%)	Structure parameter, S (μm)
TFC-S-1	0.93±0.21	1.87±0.70	40±1	553.3±43.0
TFC-S-2	0.56±0.0	0.52±0.03	59±1	375.7±7.9
TFC-D-1	0.40±0.08	0.21±0.02	71±3	1075.4±151.0
TFC-D-2	0.52±0.04	0.21±0.08	77±6	1370.7±187.2
HTI	0.12	0.19	46	1112.3

Note: The error bars were calculated based on 2–3 independent replicate tests.

with model foulants in both DS and FS. The water flux development profiles are shown in Fig. 6(a). The process included three stages: the first stage without foulants, the second stage with foulants, and the third stage without foulants after a simple crossflow wash with DI water.

In the fouling stage, all the membranes exhibited an initial decrease in water flux due to the rapid adhesion of SA on the clean membrane surface, followed by a steady drop thereafter. Among them, TFC-D-1 showed better water flux stability and better antifouling performance owing to its smoother membrane surface. The water flux in TFC-S-1 and TFC-S-2 dropped rapidly as due to the highly rough surface patterns, it was easier to adhere to dirt.

Figure 6(b) shows the selectivity of all the membranes, represented by J_S/J_V , in the three stages. Compared with TFC-S-1 and TFC-2, TFC-D-1 and TFC-D-2 had lower J_S/J_V values in all three stages, primarily due to the highly rejected PA layer that formed on the nanofibre interlayer with tiny fibres, as evidenced in Section 3.2. The nanofibre interlayer can maintain the selectivity of the membrane during operation and cleaning. During the fouling testing stage, the water flux of TFC-D-1 could be effectively improved without sacrificing the J_S/J_V value. It should be noted that the commercial HTI membranes excelled all the fabricated membranes in selectivity stability during cleaning, with a negligible change in J_S/J_V values after cleaning.

After the 5 h SA fouling test, TFC-S, TFC-D, and commercial HTI were cleaned with DI water. The surface morphology, characterised by FESEM, is shown in Fig. 7. The PA surface was contaminated with SA, and the nanofibrous substrate was less attached to the SA. The PA

layer on the coarse fibre was rough, and the foulants were more easily trapped in the dead zones (as indicated by the yellow area) of the membrane surface and were difficult to wash using water flow. In contrast, the commercial HTI membrane surface was much smoother than the PA layer, making it difficult to adhere to foulants and easy to clean. The nanofibrous substrate demonstrated its priority in mitigating fouling as the foulants were less prone to be trapped inside the pores. This was because the nanofibrous substrate had an active and interconnected open pore structure that was much larger than that of the foulants.

Additionally, NaCl played an essential role in the structural changes in the alginate fouling layer. The SA molecular chains with low NaCl content were sparse, while the SA molecular chains with high NaCl content were parallel and compact (Teng et al., 2021). Figure 8 illustrates the possible mechanism of the fouling behaviour. The higher reverse salt flux of the TFC-S membranes induced the formation of a highly cross-linked SA gel layer in the FS side, simultaneously leading to the aggravation of membrane fouling. In contrast, the dense polyamide layer of TFC-D hindered the passage of solutes and simultaneously reduced membrane fouling in the FS side.

A previous study reported a strong correlation between organic fouling and intermolecular adhesion force, and foulant-foulant interactions also played an essential role in determining the rate and extent of organic fouling (Mi and Elimelech, 2008). We used the most superior membrane (TFC-D-1) and two typical foulants, SA and BSA, to further investigate the influence of the pore structure on membrane fouling with foulants in FS and DS,

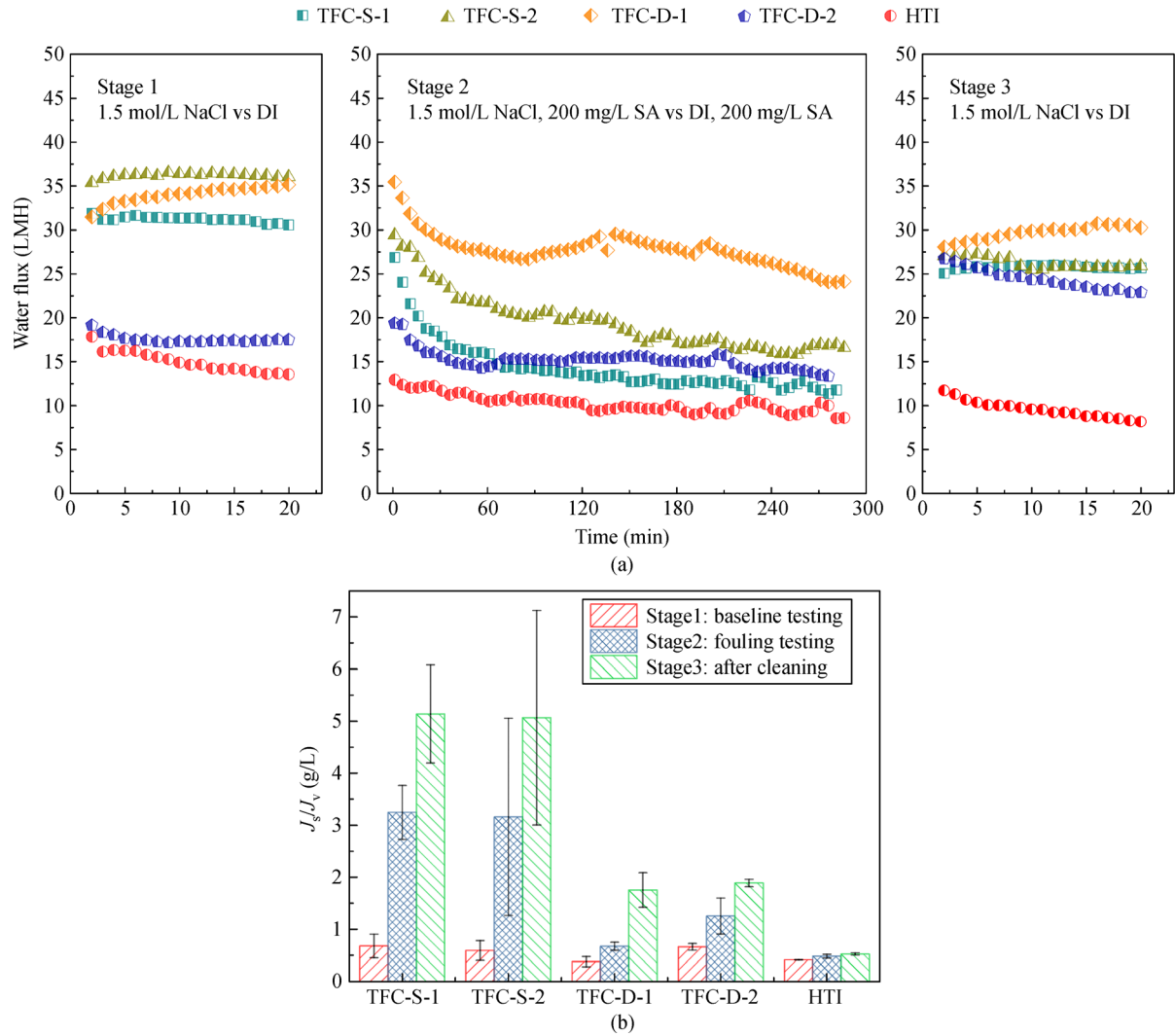


Fig. 6 (a) J_w and (b) J_s/J_v of commercial HTI and prepared membranes in the AL-DS mode. The experiment consisted of three phases: baseline test, fouling test, and after cleaning. Operating conditions: DS, 1.5 mol/L NaCl; FS, DI water; physical cleaning; foulants, 200 mg/L SA in FS and DS. The error bars were calculated based on two independent replicate tests.

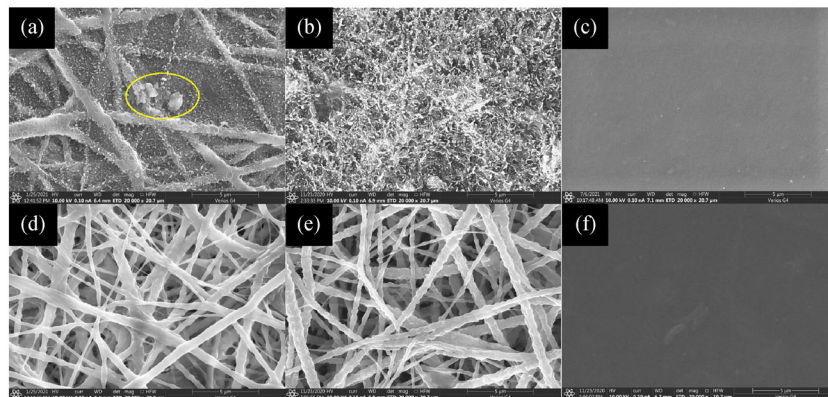


Fig. 7 FESEM images revealing the status after cleaning, the active surfaces of (a) TFC-S; (b) TFC-D; and (c) HTI and the supporting surfaces of (d) TFC-S; (e) TFC-D; and (f) HTI. The back support was imaged after peeling off the non-woven support; the marked yellow area indicates the foulants trapped in the dead zones.

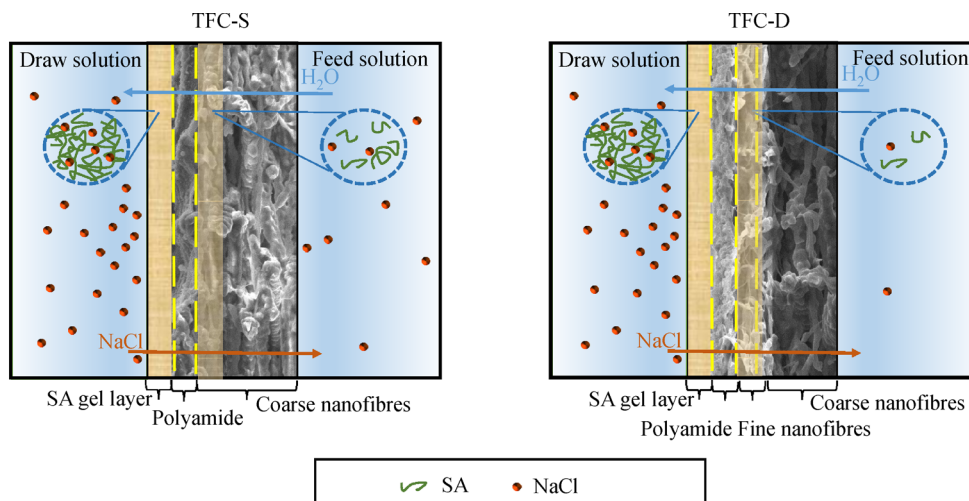


Fig. 8 Schematic of the mechanism of membrane fouling for the TFC-S and TFC-D of SA existing in both the FS and DS in the AL-DS mode.

respectively. The normalised water flux versus time is shown in Fig. 9. Each group of experiments was repeated thrice, and the results are shown in Figs. S2 and S3. It can be seen that the decline in flux caused by BSA fouling was relatively stable. In other words, SA with more vital intermolecular interactions could more easily control the development of a fouling layer on the membrane surface in a solution containing NaCl. In addition, after physical cleaning, we observed that the FRR caused by BSA was $88.5\% \pm 2.3\%$, but the FRR caused by SA was $78.1\% \pm 8.3\%$. Therefore, we speculated that compared with BSA, which had a weaker intermolecular force, the membrane surface pollution caused by SA was more severe and could not be recovered easily by physical cleaning.

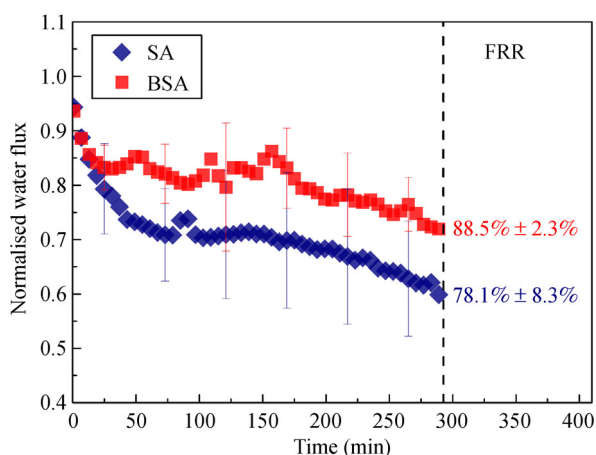


Fig. 9 Normalised water flux for TFC-D-1 after fouling testing and cleaning. The error bars were calculated based on three independent replicate tests.

We further characterised the amount of residual foulants attached to the membrane surface after physical cleaning,

and the TOC results are shown in Table 4. The amount of SA on the surface of TFC-D was 3.7 times that of BSA, indicating that SA developed more severe fouling on the membrane surface. Additionally, the SA content of TFC-S was higher than that of TFC-D, which was consistent with the FO flux test, in which the flux decline of TFC-S was more significant than that of TFC-D. This also showed that the relatively dense and antifouling PA layer of TFC-D could reduce the highly cross-linked SA gel layer caused by the higher reverse salt flux. This showed that the attached SA foulants on the commercial HTI were relatively lower than those on the TFC membranes, owing to their high hydrophilicity and smoother surface.

Table 4 Attached amount of foulants on the membrane surface

Sample code	$\rho(\text{TOC})$ (mg/cm^2)
SA (HTI)	0.004
SA (TFC-S)	0.037
SA (TFC-D)	0.011
BSA (HTI)	0.004
BSA (TFC-D)	0.003

4 Conclusions

In this study, a tiered PVDF nanofibre substrate with an ultrathin ($\sim 1 \mu\text{m}$) fine fibre interlayer on top (average fibre diameter 40–60 nm) was successfully fabricated by electrospinning. A PA selective layer was synthesised using IP on an aforesaid nanofibrous substrate with various physicochemical properties. The current study shows that the fine fibre interlayer promotes the formation of a dense and defect-free PA layer. The TFC-D-1 membrane achieved a flux of 30.2 LMH and J_s/J_v as low as 0.3 g/L using 1.5 mol/L NaCl against DI water in the AL-DS

mode. The open and interconnected pore structure without dead pores of the nanofibrous substrate effectively reduced ICP and membrane fouling, where foulants existed in both FS and DS.

This study demonstrates the importance of the interlayer in improving the TFC FO membrane. The interlayer enhanced the selectivity of the PA layer during long-term operation and cleaning. However, the current nanofibrous substrate TFC membrane was still less robust than the commercial HTI membranes during cleaning. It is suggested that more attention should be paid to membrane stability and separation performance in the future.

Conflicts of Interest There are no conflicts to declare.

Acknowledgements The authors gratefully acknowledge the National Natural Science Foundation of China (No. 52100105), the Natural Science Foundation of Shaanxi Province (China) (No. 2021JQ-108). The authors would like to thank the Singapore Membrane Technology Center of Nanyang Technological University for supporting pore size characterization.

Electronic Supplementary Material Supplementary material is available in the online version of this article at <https://doi.org/10.1007/s11783-022-1550-7> and is accessible for authorized users.

References

- Abdullah N, Yusof N, Ismail A F, Lau W J (2021). Insights into metal-organic frameworks-integrated membranes for desalination process: A review. *Desalination*, 500: 114867
- Ali A, Tufa R A, Macedonio F, Curcio E, Drioli E (2018). Membrane technology in renewable-energy-driven desalination. *Renewable & Sustainable Energy Reviews*, 81: 1–21
- Blandin G, Ferrari F, Lesage G, Le-Clech P, Héran M, Martinez-Lladó X (2020). Forward osmosis as concentration process: Review of opportunities and challenges. *Membranes (Basel)*, 10(10): 284
- Cath T, Childress A, Elimelech M (2006). Forward osmosis: Principles, applications, and recent developments. *Journal of Membrane Science*, 281(1–2): 70–87
- Deng L, Wang Q, An X, Li Z, Hu Y (2020). Towards enhanced antifouling and flux performances of thin-film composite forward osmosis membrane via constructing a sandwich-like carbon nanotubes-coated support. *Desalination*, 479: 114311
- Extrand C W (2002). Water contact angles and hysteresis of polyamide surfaces. *Journal of Colloid and Interface Science*, 248(1): 136–142
- Extrand C W (2004). Contact angles and their hysteresis as a measure of liquid-solid adhesion. *Langmuir*, 20(10): 4017–4021
- Gao F, Wang J, Zhang H, Hang M A, Cui Z, Yang G (2017). Interaction energy and competitive adsorption evaluation of different NOM fractions on aged membrane surfaces. *Journal of Membrane Science*, 542: 195–207
- Holmes-Farley S R, Reamey R H, McCarthy T J, Deutch J, Whitesides G M (1985). Acid-base behavior of carboxylic acid groups covalently attached at the surface of polyethylene: The usefulness of contact angle in following the ionization of surface functionality. *Langmuir*, 1 (6): 725–740
- Jones E, Qadir M, van Vliet M T H, Smakhtin V, Kang S M (2019). The state of desalination and brine production: A global outlook. *Science of the Total Environment*, 657: 1343–1356
- Kim L H, Bucs S S, Witkamp G J, Vrouwenvelder J S (2020). Organic composition in feed solution of forward osmosis membrane systems has no impact on the boron and water flux but reduces scaling. *Journal of Membrane Science*, 611: 118306
- Klaysom C, Hermans S, Gahlaut A, Van Craenenbroeck S, Vankelecom I F J (2013). Polyamide/Polyacrylonitrile (PA/PAN) thin film composite osmosis membranes: Film optimization, characterization and performance evaluation. *Journal of Membrane Science*, 445: 25–33
- Lau W J, Ismail A F, Misdan N, Kassim M A (2012). A recent progress in thin film composite membrane: A review. *Desalination*, 287: 190–199
- Li H, Fu M, Wang S Q, Zheng X, Zhao M, Yang F, Tang C Y, Dong Y (2021a). Stable Zr-based metal-organic framework nanoporous membrane for efficient desalination of hypersaline water. *Environmental Science & Technology*, 55(21): 14917–14927
- Li R, Li J, Rao L, Lin H, Shen L, Xu Y, Chen J, Liao B Q (2021b). Inkjet printing of dopamine followed by UV light irradiation to modify mussel-inspired PVDF membrane for efficient oil-water separation. *Journal of Membrane Science*, 619: 118790
- Liu Q, Li J, Zhou Z, Xie J, Lee J Y (2016). Hydrophilic mineral coating of membrane substrate for reducing internal concentration polarization (ICP) in forward osmosis. *Scientific Reports*, 6(1): 19593
- Luo F, Wang J, Yao Z, Zhang L, Chen H (2021). Polydopamine nanoparticles modified nanofiber supported thin film composite membrane with enhanced adhesion strength for forward osmosis. *Journal of Membrane Science*, 618: 118673
- Manju S, Sagar N (2017). Renewable energy integrated desalination: A sustainable solution to overcome future fresh-water scarcity in India. *Renewable & Sustainable Energy Reviews*, 73: 594–609
- Martinetti C R, Childress A E, Cath T Y (2009). High recovery of concentrated RO brines using forward osmosis and membrane distillation. *Journal of Membrane Science*, 331(1–2): 31–39
- McCutcheon J R, Elimelech M (2006). Influence of concentrative and dilutive internal concentration polarization on flux behavior in forward osmosis. *Journal of Membrane Science*, 284(1–2): 237–247
- Mi B, Elimelech M (2008). Chemical and physical aspects of organic fouling of forward osmosis membranes. *Journal of Membrane Science*, 320(1–2): 292–302
- Nasrul A, Bastian A, Sri M, Yoshikage O, Hideto M (2011). Improved fouling reduction of PES hollow fiber membranes by incorporation with non-ionic surfactant. *Research Journal of Chemistry and Environment*, 15(2): 212–216
- Park M J, Gonzales R R, Abdel-Wahab A, Phuntsho S, Shon H K (2018). Hydrophilic polyvinyl alcohol coating on hydrophobic electrospun nanofiber membrane for high performance thin film composite forward osmosis membrane. *Desalination*, 426: 50–59
- Peng L E, Yao Z, Yang Z, Guo H, Tang C Y (2020). Dissecting the role of substrate on the morphology and separation properties of thin film composite polyamide membranes: seeing is believing. *Environmental Science & Technology*, 54(11): 6978–6986
- Qasim M, Darwish N A, Sarp S, Hilal N (2015). Water desalination by forward (direct) osmosis phenomenon: A comprehensive review. *Desalination*, 374: 47–69

- Saleem H, Trabzon L, Kilic A, Zaidi S J (2020). Recent advances in nanofibrous membranes: Production and applications in water treatment and desalination. *Desalination*, 478: 114178
- Sreedhar I, Khaitan S, Gupta R, Reddy B M, Venugopal A (2018). An odyssey of process and engineering trends in forward osmosis. *Environmental Science. Water Research & Technology*, 4(2): 129–168
- Suwaileh W, Johnson D, Hilal N (2020). Membrane desalination and water re-use for agriculture: State of the art and future outlook. *Desalination*, 491: 114559
- Tang C Y, Yang Z, Guo H, Wen J J, Nghiem L D, Cornelissen E (2018). Potable water reuse through advanced membrane technology. *Environmental Science & Technology*, 52(18): 10215–10223
- Teng J H, Zhang H M, Tang C Y, Lin H J (2021). Novel molecular level insights into forward osmosis membrane fouling affected by reverse diffusion of draw solutions based on thermodynamic mechanisms. *Journal of Membrane Science*, 620: 118815
- Tian M, Qiu C, Liao Y, Chou S, Wang R (2013). Preparation of polyamide thin film composite forward osmosis membranes using electrospun polyvinylidene fluoride (PVDF) nanofibers as substrates. *Separation and Purification Technology*, 118: 727–736
- Tian M, Wang R, Goh K, Liao Y, Fane A G (2015). Synthesis and characterization of high-performance novel thin film nanocomposite PRO membranes with tiered nanofiber support reinforced by functionalized carbon nanotubes. *Journal of Membrane Science*, 486: 151–160
- Tian M, Wang Y N, Wang R, Fane A G (2017). Synthesis and characterization of thin film nanocomposite forward osmosis membranes supported by silica nanoparticle incorporated nanofibrous substrate. *Desalination*, 401: 142–150
- Wang H, Gao B, Hou L A, Shon H K, Yue Q, Wang Z (2021). Fertilizer drawn forward osmosis as an alternative to 2nd pass seawater reverse osmosis: Estimation of boron removal and energy consumption. *Frontiers of Environmental Science & Engineering*, 15(6): 135
- Wang J, Dlamini D S, Mishra A K, Pendergast M T M, Wong M C Y, Mamba B B, Freger V, Verliefe A R D, Hoek E M V (2014). A critical review of transport through osmotic membranes. *Journal of Membrane Science*, 454: 516–537
- Wang R, Shi L, Tang C Y Y, Chou S R, Qiu C, Fane A G (2010). Characterization of novel forward osmosis hollow fiber membranes. *Journal of Membrane Science*, 355(1–2): 158–167
- Wang Y, Zhang M K, Liu Y Q, Xiao Q Q, Xu S C (2016). Quantitative evaluation of concentration polarization under different operating conditions for forward osmosis process. *Desalination*, 398: 106–113
- Wenzel R N (1949). Surface roughness and contact angle. *Journal of Physical and Colloid Chemistry*, 53(9): 1466–1467
- Xiao K, Liang S, Wang X, Chen C, Huang X (2019). Current state and challenges of full-scale membrane bioreactor applications: A critical review. *Bioresource Technology*, 271: 473–481
- Xu W X, Chen Q Z, Ge Q C (2017). Recent advances in forward osmosis (FO) membrane: Chemical modifications on membranes for FO processes. *Desalination*, 419: 101–116
- Xue W, Zaw M, An X, Hu Y, Tabucanon A S (2020). Sea salt bittern-driven forward osmosis for nutrient recovery from black water: A dual waste-to-resource innovation via the osmotic membrane process. *Frontiers of Environmental Science & Engineering*, 14(2): 32
- Yadav S, Saleem H, Ibrar I, Naji O, Hawari A A, Alanezi A A, Zaidi S J, Altaee A, Zhou J (2020). Recent developments in forward osmosis membranes using carbon-based nanomaterials. *Desalination*, 482: 114375
- Yang Z, Guo H, Tang C Y Y (2019). The upper bound of thin-film composite (TFC) polyamide membranes for desalination. *Journal of Membrane Science*, 590: 117297
- Yang Z, Sun P F, Li X, Gan B, Wang L, Song X, Park H D, Tang C Y (2020). A critical review on thin-film nanocomposite membranes with interlayered structure: mechanisms, recent developments, and environmental applications. *Environmental Science & Technology*, 54(24): 15563–15583
- Yu F Y, Shi H T, Shi J, Teng K Y, Xu Z W, Qian X M (2020). High-performance forward osmosis membrane with ultra-fast water transport channel and ultra-thin polyamide layer. *Journal of Membrane Science*, 616: 118611
- Zhang K M, An X C, Bai Y, Shen C, Jiang Y P, Hu Y X (2021). Exploration of food preservatives as draw solutes in the forward osmosis process for juice concentration. *Journal of Membrane Science*, 635: 119495
- Zhang M, Jin W, Yang F, Duke M, Dong Y, Tang C Y Y (2020). Engineering a nanocomposite interlayer for a novel ceramic-based forward osmosis membrane with enhanced performance. *Environmental Science & Technology*, 54(12): 7715–7724
- Zhang S, Wang K Y, Chung T S, Chen H M, Jean Y C, Amy G (2010). Well-constructed cellulose acetate membranes for forward osmosis: Minimized internal concentration polarization with an ultra-thin selective layer. *Journal of Membrane Science*, 360(1–2): 522–535
- Zhang X, Xiong S, Liu C X, Shen L, Ding C, Guan C Y, Wang Y (2019). Confining migration of amine monomer during interfacial polymerization for constructing thin-film composite forward osmosis membrane with low fouling propensity. *Chemical Engineering Science*, 207: 54–68
- Zhou Z Y, Hu Y X, Boo C, Liu Z Y, Li J Q, Deng L Y, An X C (2018). High-performance thin-film composite membrane with an ultrathin spray-coated carbon nanotube interlayer. *Environmental Science & Technology Letters*, 5(5): 243–248